PCSMC Design of Permanent Magnetic Synchronous Generator for Maximum Power Point Tracking

Bo Yang [1], Linen Zhong [1], Tao Yu [2,*], Hongchun Shu [1], Pulin Cao [1], Na An [1], Yiyan Sang [3], and Lin Jiang [3]

[1] Faculty of Electric Power Engineering, Kunming University of Science and Technology, 650500 Kunming, China;
[2] College of Electric Power, South China University of Technology, 510640 Guangzhou, China;
[3] Department of Electrical Engineering & Electronics, University of Liverpool, Liverpool, L69 3GJ, United Kingdom;
* Correspondence: taoyu1@scut.edu.cn, Tel.: +86-130-020-88518

Abstract: This paper develops a perturbation compensation based sliding-mode control (PCSMC) strategy of a permanent magnetic synchronous generator (PMSG) for optimal extraction of wind energy. Firstly, PMSG nonlinearities, uncertain parameters, unmodelled dynamics, and stochastic wind speed variations are aggregated into a perturbation. Then, it is estimated by a sliding-mode state and perturbation observer (SMSPO) in the real-time. Further, the perturbation estimate is fully cancelled by sliding-mode controller (SMC) for global control consistency, together with considerable robustness thanks to the sliding-mode mechanism. In addition, the upper bound of perturbation is replaced by its real-time estimate, thus more proper control costs could be achieved without over-conservativeness. Moreover, PCSMC does not require an accurate PMSG model while only the measurement of d-axis current and mechanical rotation speed is required. Four case studies are carried out, e.g., step change of wind speed, low-turbulence stochastic wind speed, high-turbulence stochastic wind speed, and PMSG parameter uncertainties. Simulation results demonstrate that PCSMC can rapidly extract higher power under different wind speed profiles against vector control (VC) and SMC. Lastly, a dSpace based hardware-in-the-loop (HIL) experiment is undertaken which validates its implementation feasibility.

Keywords: PMSG; perturbation compensation based sliding-mode control; MPPT; perturbation observer

Nomenclature

Variables		***Abbreviations***	
v_{wind}	wind velocity	**MPPT**	maximum power point tracking
ρ	air density	**PMSG**	permanent magnetic synchronous generator
C_P	power coefficient	**VC**	vector control
λ	tip-speed-ratio	**SMSPO**	sliding-mode state and perturbation observer
β	blade pitch angle	**SMC**	sliding-mode control
T_e	electromagnetic torque	**SPWM**	sinusoidal pulse width modulation
T_m	mechanical torque	**VSC**	voltage source converter
ω_e	electrical rotation speed	**PID**	proportional-integral-derivative
ω_m	mechanical rotation speed of turbine	**FLC**	feedback linearization control
V_d, V_q	dq-axis stator voltages	**PCSMC**	perturbation compensation based sliding-mode control
i_d, i_q	dq-axis currents	**SMPO**	sliding-mode perturbation observer
System parameters		***The control parameters of PCSMC***	
L_d, L_q	dq-axis inductances	γ_1, γ_2	positive constants
p	the number of pole pairs	α_i	Luenberger observer gains
R	turbine radius	ρ_i	estimated sliding surface gains
J_{tot}	total inertia of the drive train	φ_i, ς_i	sliding-mode control gains
D	viscous damping coefficient	ϵ_c, ϵ_o	thickness layer boundary of controller and observer
R_s	stator resistance	B_0	constant control gain

1. Introduction

Environmental concerns in energy generation from the conventional sources have driven rapid development of renewable energy sources (RES) around the globe, including wind, solar, fuel cell, hydro, tidal, geothermal, biomass, etc. Meanwhile, the ever-increasing social and industrial demand for electrical energy and the issues associated with limited reserves and the rising costs of conventional fossil fuels, e.g., coal, natural gas, and oil, etc., have urgently driven the worldwide deployment of renewable energy [1,2]. At present, wind energy conversion system (WECS) has become quite popular thanks to its cleanness, abundance of resources, as well as wide distribution [3]. So far, there are two major wind generators, e.g., doubly-fed induction generator (DFIG) [4] and permanent magnetic synchronous generator (PMSG) [5]. Recently, PMSG applications have been significantly growing due to its prominent characteristics of efficient energy production, gearless construction, simple structure, as well as self-excitation [6].

In general, one of the most crucial objective of PMSG operation is to extract the optimal wind power under different operation conditions, which is often denoted as maximum power point tracking (MPPT) [7]. In order to achieve this goal, an appropriate control system design is very important. Conventional vector control (VC) scheme employing proportional-integral-derivative (PID) framework is commonly employed in industry thanks to its reliability and simplicity [8]. Nevertheless, PID control performance might be dramatically degraded or even result in a collapse of system stability when operation conditions vary as the its control parameters are merely based on one-point linearization, such issue becomes even severer in PMSGs as they usually have strong nonlinearity caused by wind turbines aerodynamics, converters, as well as the inherent nature of wind, e.g., intermittence and randomness. Hence, more advanced controllers are needed for PMSG to tackle the above thorny obstacle.

Thus far, there are mainly two types of methodology being adopted for the aforementioned issue, that is, meta-heuristic optimization algorithms and nonlinear robust/adaptive approaches. The former one is inspired from the biological evolution or swarm-based algorithm [9]. It usually constructs a fitness function consisted of the tracking error of controlled variables, and adjusts the control parameters to achieve an optimal control performance via minimizing the fitness function. Genetic algorithm (GA) was utilized to tune PI control parameters of PMSG system with both symmetrical and unsymmetrical faults [10]. Moreover, particle swarm optimization (PSO) was adopted to enhance the optimal power tracking rate of PMSG in the presence of severe wind speed variations by investigating the participation factors of state variables, which simplifies the problem by reducing the number of PI control parameters needed to be tuned [11]. In addition, firefly algorithms (FA) was employed to seek the optimal PID parameters of pitch angle regulator which realizes a stable and optimal power tracking [12].

Alternatively, the latter one attempts to design nonlinear robust/adaptive controllers to resolve this difficult challenge by studying PMSG or wind characteristics. Reference [13] proposed feedback linearization control (FLC) to completely compensate all PMSG nonlinearities, which however requires an accurate system model and lack robustness against any modelling uncertainties. Besides, a digital robust H_∞ control was designed to handle stochastic wind speed variations and generator parameter uncertainties [14]. Additionally, [15] reported an improved adaptive torque gain (IATG) method of PMSG which customizes adaptive torque gains and enhances MPPT performances. Besides, a modified perturbation and observation (P&O) MPPT algorithm was applied to accomplish a fast tracking of the maximum power point (MPP) under a rapidly changing of the wind speed, which requires neither the knowledge of wind turbine system parameters nor mechanical sensors [16]. In [17], a model predictive control (MPC) was proposed, which can predict the future behaviour of PMSG. Furthermore, nonlinear Luenberger observer based control was developed for unknown PMSG parameters or variables estimation [18].

Among the enormous variety of nonlinear robust/adaptive methods, sliding-mode control (SMC) provides a powerful tool to handle uncertainties and disturbances via high-frequency switching mechanism, which is based on variable structure control and owns elegant merits of fast response, implementation simplicity, robustness improvement, as well as disturbance suppression [19]. Hence, it has been widely employed on PMSG, e.g., a fuzzy integral SMC was presented for MPPT with an additional goal of eliminating high-order voltage harmonics [20]. In addition, an SMC using enhanced exponential reaching law was developed to attenuate chattering [21]. Moreover, high-order SMC strategy was adopted for rapid active and reactive power regulation, as well as minimizes the generation losses [22]. Besides, [23] reported a discrete-time integral SMC with a chattering free reaching law of PMSG to realize MPPT under various wind speed. Further, in [24], a modified version of the super-twisting algorithm with variable gains was incorporated with SMC to effectively reject the variation on the parameters and the random nature of wind speed. Additionally, sliding mode model reference adaptive system (SM-MRAS) speed observer based fuzzy controller was devised [25], which provides considerable robustness.

However, one obvious drawback of SMC is the inherent over-conservativeness resulted from the use of upper bound of uncertainties, while such conditions, e.g., perturbation takes its upper bound, are not frequently appeared. Therefore, it motivates the authors to design a modified SMC scheme through perturbation compensation. The reason to design PCSMC and its advantages can be summarized as follows:

- As PMSG always operate under various uncertainties, an effective adaptive control scheme is urgently needed to achieve a satisfactory MPPT performance. It motivates this paper to design PCSMC to aggregate the combinatorial effect of generator nonlinearities and parameter uncertainties, unmodelled dynamics, and wind speed randomness into a perturbation, which is rapidly estimated by a sliding-mode state and perturbation observer (SMSPO) in real-time. Thus, PCSMC can effectively tackle various types of uncertainties which is applicable to more practical cases compared to that of other parameter estimation based methods;
- Compared to conventional PID control [8], PCSMC can achieve a global control consistency under various operation conditions as all PMSG nonlinearities are globally removed;
- Compared to FLC [13], an accurate PMSG model is not needed by PCSMC, thus a great robustness could be realized via real-time perturbation compensation. Therefore, PCSMC is easy for practical implementation;
- Compared to conventional SMC [22], upper bound of perturbation is replaced by its real-time estimate in PCSMC, such that an improved tracking accuracy and proper control costs are achieved.

2. Modelling of PMSG System

Figure 1 demonstrates the structure of PMSG system. Here, active/reactive power is controlled by generator-side voltage source converter (VSC), while grid-side VSC transmits active power to main power grid through DC-link capacitor [13].

2.1. PMSG modelling

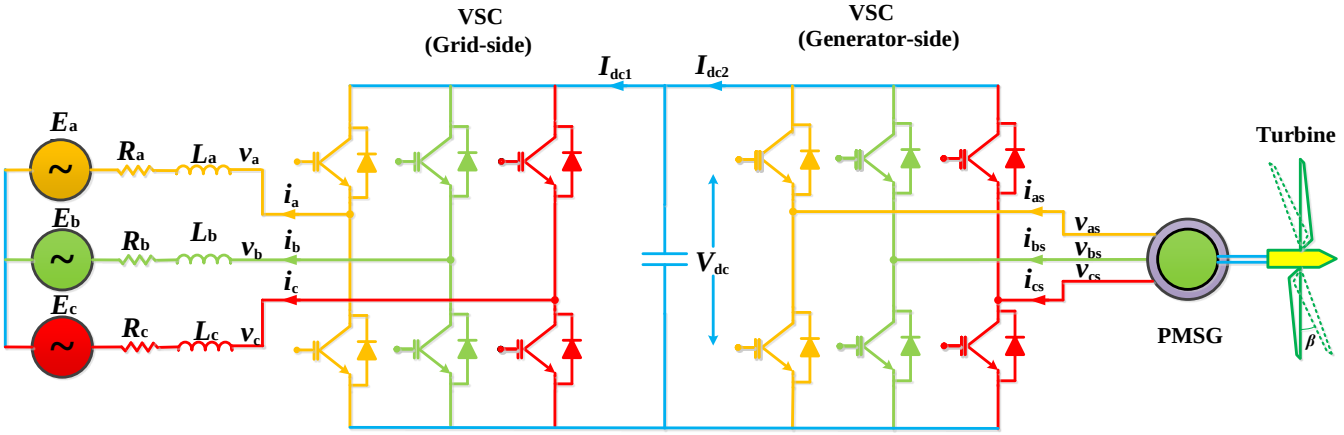

Fig. 1 *The configuration of a PMSG system.*

The wind turbine aerodynamics is modelled by power coefficient $C_p(\lambda,\beta)$, which includes tip-speed-ratio λ and blade pitch angle β, with λ being defined as follows

$$\lambda = \frac{\omega_m R}{v_{wind}} \tag{1}$$

where ω_m is the mechanical rotation speed and v_{wind} denotes the wind speed; R denotes the blade radius, respectively. In particular, power coefficient $C_p(\lambda,\beta)$ can be described by

$$C_p(\lambda,\beta) = c_1\left(\frac{c_2}{\lambda_i} - c_3\beta - c_4\right)e^{-\frac{c_5}{\lambda_i}} \tag{2}$$

with

$$\frac{1}{\lambda_i} = \frac{1}{\lambda+0.08\beta} - \frac{0.035}{\beta^3+1} \tag{3}$$

where the coefficients c_1 to c_5 are selected as c_1=0.22, c_2=116, c_3=0.4, c_4=5, and c_5=12.5, respectively [13,26].

Besides, mechanical power is calculated by

$$P_m = \frac{1}{2}\rho\pi R^2 C_p(\lambda,\beta)v_{wind}^3 \tag{4}$$

where ρ represents the air density.

The dynamics of PMSG and shaft system can be found in references [13,26].

2.2. *MPPT profile*

For MPPT, power coefficient $C_p(\lambda,\beta)$ must be kept at maximum point C_p^* under different wind profiles, yields

$$C_p^* = C_p(\lambda^*) \tag{5}$$

Thus, mechanical rotation speed ω_m should be regulated to track the optimal rotation speed ω_m^* as

$$\omega_m^* = \frac{v_{wind}}{R}\lambda^* \tag{6}$$

Here, the pitch angle $\beta = 2°$ while optimal tip-speed-ratio $\lambda^* = 7$, thus one can readily obtain $C_p^* = 0.4019$ [13,26].

Lastly, Figure 2 shows the optimal active power curve under different wind profile [27,28], as follows

$$P_{opt}(\omega_m) = K^*\omega_m^3 \tag{7}$$

where $K^* = 0.5\rho\pi R^5 C_p^*/(\lambda^*)^3$ is the shape coefficient.

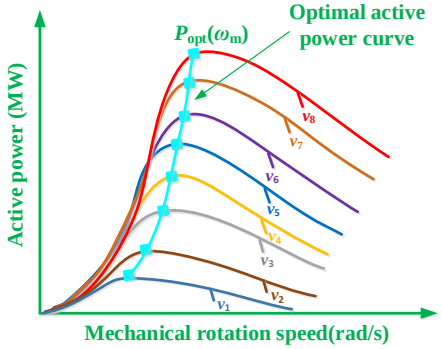

Fig. 2 *The MPPT profile obtained at various wind speeds.*

3. Perturbation Compensation based Sliding-mode Control

Consider a canonical uncertain nonlinear system

$$\begin{cases}\dot{x} = Ax + B(a(x) + b(x)u + d(t)) \\ y = x_1\end{cases} \tag{8}$$

where $x = [x_1, x_2, \cdots, x_n]^T \in R^n$ represents state variable vector; $u \in R$ and $y \in R$ are control input and system output, respectively; $a(x)$: $R^n \mapsto R$ and $b(x)$: $R^n \mapsto R$ are unknown smooth functions; and $d(t)$: $R^+ \mapsto R$ represents time-varying external disturbances.

The perturbation of system (8) is defined as [29-32]

$$\psi(x,u,t) = a(x) + (b(x) - b_0)u + d(t) \tag{9}$$

where b_0 means the constant control gain.Here, the last state x_n can be rewritten in terms of perturbation (9), gives

$$\dot{x}_n = a(x) + (b(x) - b_0)u + d(t) + b_0u = \psi(x,u,t) + b_0u \tag{10}$$

Define a fictitious state to represent the perturbation, e.g., $x_{n+1} = \psi(x,u,t)$. Then, system (8) becomes

$$\begin{cases} y = x_1 \\ \dot{x}_1 = x_2 \\ \vdots \\ \dot{x}_n = x_{n+1} + b_0u \\ \dot{x}_{n+1} = \dot{\psi}(\cdot) \end{cases} \tag{11}$$

The new state vector becomes $x_e = [x_1, x_2, \cdots, x_n, x_{n+1}]^T$, while the following assumptions are made [30]

A.1 b_0 should satisfy: $|\boldsymbol{b(x)/b_0 - 1}| \leq \boldsymbol{\theta < 1}$, where θ is a positive constant.

A.2 The function $\boldsymbol{\psi(x,u,t)}$: $\boldsymbol{R^n \times R \times R^+ \mapsto R}$ and $\boldsymbol{\dot{\psi}(x,u,t)}$: $\boldsymbol{R^n \times R \times R^+ \mapsto R}$ are bounded over the domain of interest: $|\boldsymbol{\psi(x,u,t)}| \leq \boldsymbol{\gamma_1}$, $|\boldsymbol{\dot{\psi}(x,u,t)}| \leq \boldsymbol{\gamma_2}$ with $\boldsymbol{\psi(0,0,0) = 0}$, and $\boldsymbol{\dot{\psi}(0,0,0) = 0}$, where $\boldsymbol{\gamma_1}$ and $\boldsymbol{\gamma_2}$ are positive constants.

A.3 The desired trajectory $\boldsymbol{y_d}$ and its up to *n*th-order derivative are all continuous and bounded.

Here, assumptions **A.1** and **A.2** ensure the closed-loop system stability, while assumption **A.3** guarantees PCSMC can regulate state *x* to track the desired trajectory $x_d = [y_d, y_d^{(1)}, \cdots, y_d^{(n-1)}]^T$.

Throughout this paper, $\tilde{x} = x - \hat{x}$ refers to the estimation error of *x* whereas $\hat{x}$ represents the estimate of *x*, while *x** is the reference of *x*. Consider the worst case, e.g., $y=x_1$ is the only measurable state, an (*n*+1)th-order SMSPO for the extended system (17) is employed to simultaneously estimate the system states and perturbation, as follows [29-32]:

$$\begin{cases} \dot{\hat{x}}_1 = \hat{x}_2 + \alpha_1\tilde{x}_1 + k_1\text{sat}(\tilde{x}_1, \epsilon_o) \\ \vdots \\ \dot{\hat{x}}_n = \hat{\psi}(\cdot) + \alpha_n\tilde{x}_1 + k_n\text{sat}(\tilde{x}_1, \epsilon_o) + b_0u \\ \dot{\hat{\psi}}(\cdot) = \alpha_{n+1}\tilde{x}_1 + k_{n+1}\text{sat}(\tilde{x}_1, \epsilon_o) \end{cases} \tag{12}$$

(18)

where α_i, i = 1, 2,⋯, n + 1, are the Luenberger observer gains, which are chosen to place the poles of polynomial $s^{n+1} + \alpha_1 s^n + \alpha_2 s^{n-1} + \cdots + \alpha_{n+1} = (s + \lambda_\alpha)^{n+1} = 0$ being in the open left-half complex plane at $-\lambda_\alpha$, with

$$\alpha_i = C_{n+1}^i \lambda_\alpha^i, i = 1,2,\cdots,n+1. \tag{13}$$

Besides, positive gains k_i are sliding surface constants, which satisfies

$$k_1 \geq |\tilde{x}_2|_{\max} \tag{14}$$

where the ratio k_i/k_1 (i = 2, 3,⋯, n + 1) are chosen to assign the poles of $p^n + (k_2/k_1)p^{n-1} + \cdots + (k_n/k_1)p + (k_{n+1}/k_1) = (p + \lambda_k)^n = 0$ to be in the open left-half complex plane at $-\lambda_k$, yields

$$\frac{k_{i+1}}{k_1} = C_n^i \lambda_k^i, \ i = 1,2,\cdots,n. \tag{15}$$

with $C_n^i = \frac{n!}{i!(n-i)!}$.

Moreover, sat$(\tilde{x}_1, \epsilon_o)$ function is adopted to replace the conventional sgn$(\tilde{x}_1)$ function to attenuate the malignant effect of chattering in SMSPO, which is defined as sat$(\tilde{x}_1, \epsilon_o) = \tilde{x}_1/|\tilde{x}_1|$ when$|\tilde{x}_1| > \epsilon_o$ and sat $(\tilde{x}_1, \epsilon_o) = \tilde{x}_1/\epsilon_o$ when $|\tilde{x}_1| \leq \epsilon_o$. In addition, ϵ_o means the thickness layer boundary of observer.

Define the estimated sliding surface as

$$\hat{S}(x,t) = \sum_{i=1}^n \rho_i \left(\hat{x}_i - y_d^{(i-1)}\right) \tag{16}$$

where the estimated sliding surface gains $\rho_i = C_{n-1}^{i-1}\lambda_c^{n-i}, i = 1,\cdots,n$, place all poles of the estimated sliding surface at -λ_c, with $\lambda_c > 0$.

To this end, the PCSMC for system (13) is designed as $u = \frac{1}{b_0}[y_d^{(n)} - \sum_{i=1}^{n-1}\rho_i(\hat{x}_{i+1} - y_d^{(i)}) - \varsigma\hat{S} - \varphi\text{sat}(\hat{S}, \epsilon_c) - \hat{\psi}(\cdot)]$ (17)

where ς and φ are sliding-mode control gains which are chosen to fulfil the attractiveness of the estimated sliding surface $\hat{S}$. In addition, ϵ_c is the thickness layer boundary of controller.

Remark 1. *In conventional SMC, upper bound of perturbation is employed to determine the control gain, which often leads to over-conservativeness. Actually, such extreme condition, e.g., the perturbation takes its upper bound, is quite rare. In contrast, PCSMC only uses the upper bound of perturbation in the observer loop, hence the tracking performance can be enhanced with more proper control costs.*

The overall PCSMC design for system (8) can be summarized as

Step 1: Define perturbation (9) for the original *n*th-order system (8);

Step 2: Define a fictitious state $x_{n+1} = \psi(\cdot)$ to represent perturbation (9);

Step 3: Extend the original *n*th-order system (8) into the extended (*n*+1)th-order system (11);

Step 4: Use the (*n*+1)th-order SMSPO (12) for the extended (*n*+1)th-order system (11) to obtain the state estimate $\hat{x}$ and the perturbation estimate $\hat{\psi}(\cdot)$ by the only measurement of x_1;

Step 5: Design PCSMC for the original *n*th-order system (8), in which the estimated sliding surface $\hat{S}$ is calculated by (16).

4. PCSMC Design of PMSG for MPPT

Define state variable $\Omega = [i_d, i_q, \omega_m]^T$ and output $Y = [y_1, y_2]^T = [i_d, \omega_m]^T$, the state space equation is written as

$$\dot{\Omega} = f(x) + g_1(x)u_1 + g_2(x)u_2 \tag{18}$$

where

$$f(x) = \begin{bmatrix} -\frac{R_s}{L_d} i_d + \frac{\omega_e L_q}{L_d} i_q \\ -\frac{R_s}{L_q} i_q - \frac{\omega_e}{L_q}(L_d i_d + K_e) \\ \frac{1}{J_{tot}}(T_m - T_e) \end{bmatrix},$$

$$g_1(x) = \begin{bmatrix} \frac{1}{L_d} \\ 0 \\ 0 \end{bmatrix}, g_2(x) = \begin{bmatrix} 0 \\ \frac{1}{L_q} \\ 0 \end{bmatrix} \tag{19}$$

Differentiate output Y until control input $u = [u_1, u_2]^T = [V_d, V_q]^T$ appears explicitly, it obtains

$$\begin{cases} \dot{y}_1 = \frac{1}{L_d} u_1 - \frac{R_s}{L_d} i_d + \frac{\omega_e L_q}{L_d} i_q \\ \ddot{y}_2 = -\frac{p i_q}{J_{tot} L_d}(L_d - L_q) u_1 + \frac{\dot{T}_m}{J_{tot}} - \frac{p}{J_{tot} L_q}[K_e + (L_d - L_q) i_d] u_2 \\ \quad -\frac{p i_q}{J_{tot} L_d}(L_d - L_q)(-R_s i_d + L_q \omega_e i_q) + \\ \quad \frac{p}{J_{tot} L_q}[K_e + (L_d - L_q) i_d](L_d \omega_e i_d + R_s i_q + \omega_e K_e) \end{cases} \tag{20}$$

System (20) can then be rewritten into the following matrix form

$$\begin{bmatrix} \dot{y}_1 \\ \ddot{y}_2 \end{bmatrix} = \begin{bmatrix} h_1(x) \\ h_2(x) \end{bmatrix} + B(x) \begin{bmatrix} u_1 \\ u_2 \end{bmatrix} \tag{21}$$

where

$$h_1(x) = -\frac{R_s}{L_d} i_d + \frac{\omega_e L_q}{L_d} i_q \tag{22}$$

$$h_2(x) = \frac{\dot{T}_m}{J_{tot}} - \frac{p i_q}{J_{tot} L_q}(L_d - L_q)(-R_s i_d + L_q \omega_e i_q) + \frac{p}{J_{tot} L_q}[K_e + (L_d - L_q) i_d](L_d \omega_e i_d + R_s i_q + \omega_e K_e) \tag{23}$$

with

$$B(x) = \begin{bmatrix} \frac{1}{L_d} & 0 \\ -\frac{p i_q}{J_{tot} L_d}(L_d - L_q) & -\frac{p}{J_{tot} L_q}[K_e + (L_d - L_q) i_d] \end{bmatrix} \tag{24}$$

This input-output linearization is valid only if matrix $B(x)$ is nonsingular among the whole operation range, gives

$$\det[B(x)] = -\frac{p[K_e + (L_d - L_q) i_d]}{J_{tot} L_d L_q} \neq 0 \tag{25}$$

which can be always satisfied when $K_e \neq -(L_d - L_q) i_d$.

Define the perturbations $\psi_1(\cdot)$ and $\psi_2(\cdot)$ for system (20) as

$$\begin{bmatrix} \psi_1(\cdot) \\ \psi_2(\cdot) \end{bmatrix} = \begin{bmatrix} h_1(x) \\ h_2(x) \end{bmatrix} + (B(x) - B_0) \begin{bmatrix} u_1 \\ u_2 \end{bmatrix} \tag{26}$$ (32)

where constant control gain matrix B_0 is designed as

$$B_0 = \begin{bmatrix} b_{11} & 0 \\ 0 & b_{22} \end{bmatrix} \tag{27}$$

where b_{11} and b_{22} are constant control gains. Note that diagonal matrix B_0 is chosen to realize a fully decoupled control of d-axis current and mechanical rotation speed.

Define tracking error $e = [e_1, e_2]^T = [i_d - i_d^*, \omega_m - \omega_m^*]^T$, one can obtain

$$\begin{bmatrix} \dot{e}_1 \\ \ddot{e}_2 \end{bmatrix} = \begin{bmatrix} \psi_1(\cdot) \\ \psi_2(\cdot) \end{bmatrix} + B_0 \begin{bmatrix} u_1 \\ u_2 \end{bmatrix} - \begin{bmatrix} \dot{i}_d^* \\ \ddot{\omega}_m^* \end{bmatrix} \tag{28}$$

A second-order sliding-mode perturbation observer (SMPO) is used for perturbation $\psi_1(\cdot)$ estimation, as

$$\begin{cases} \dot{\hat{i}}_d = \hat{\psi}_1(\cdot) + \alpha_{11} \tilde{i}_d + k_{11} \mathrm{sat}(\tilde{i}_d, \epsilon_o) + b_{11} u_1 \\ \dot{\hat{\psi}}_1(\cdot) = \alpha_{12} \tilde{i}_d + k_{12} \mathrm{sat}(\tilde{i}_d, \epsilon_o) \end{cases} \tag{29}$$

where observer gains k_{11}, k_{12}, α_{11}, and α_{12}, are all positive constants.

Meanwhile, a third-order SMSPO is adopted for perturbation $\psi_2(\cdot)$ estimation, as

$$\begin{cases} \dot{\hat{\omega}}_{\mathrm{m}} = \hat{\omega}_m + \alpha_{21}\tilde{\omega}_{\mathrm{m}} + k_{21}\mathrm{sat}(\tilde{\omega}_{\mathrm{m}}, \epsilon_{\mathrm{o}}) \\ \dot{\hat{\omega}}_{\mathrm{m}} = \hat{\psi}_2(\cdot) + \alpha_{22}\tilde{\omega}_{\mathrm{m}} + k_{22}\mathrm{sat}(\tilde{\omega}_{\mathrm{m}}, \epsilon_{\mathrm{o}}) + b_{22}u_2 \\ \dot{\hat{\psi}}_2(\cdot) = \alpha_{23}\tilde{\omega}_{\mathrm{m}} + k_{23}\mathrm{sat}(\tilde{\omega}_{\mathrm{m}}, \epsilon_{\mathrm{o}}) \end{cases} \quad (30)$$

where observer gains k_{21}, k_{22}, k_{23}, α_{21}, α_{22}, and α_{23}, are all positive constants.

The estimated sliding surface is designed for system (21) as

$$\begin{bmatrix} \hat{S}_1 \\ \hat{S}_2 \end{bmatrix} = \begin{bmatrix} \hat{\imath}_{\mathrm{d}} - i_{\mathrm{d}}^* \\ \rho_1(\hat{\omega}_{\mathrm{m}}^* - \omega_{\mathrm{m}}^*) + \rho_2(\hat{\omega}_{\mathrm{m}}^* - \dot{\omega}_{\mathrm{m}}^*) \end{bmatrix} \quad (31)$$

where positive constants ρ_1 and ρ_2 represent the sliding surface gains. It is worth noting that a larger gain will lead to a faster tracking rate but also a higher control costs. In order to obtain a proper trade-off between the tracking rate and control costs, these gains values are determined through trial-and-error. The attractiveness of system (31) guarantees the convergence of d-axis current i_{d} and mechanical rotation speed ω_{m}.

Lastly, PCSMC for PMSG system (21) is designed as

$$\begin{bmatrix} u_1 \\ u_2 \end{bmatrix} = B_0^{-1} \begin{bmatrix} i_{\mathrm{d}}^* - \hat{\psi}_1(\cdot) - \varsigma_1\hat{S}_1 - \varphi_1\mathrm{sat}(\hat{S}_1, \epsilon_{\mathrm{c}}) \\ \dot{\omega}_{\mathrm{m}}^* - \hat{\psi}_2(\cdot) - \rho_1(\hat{\omega}_{\mathrm{m}}^* - \dot{\omega}_{\mathrm{m}}^*) - \varsigma_2\hat{S}_2 - \varphi_2\mathrm{sat}(\hat{S}_2, \epsilon_{\mathrm{c}}) \end{bmatrix} \quad (32)$$

where control gains ς_1, ς_2, φ_1, and φ_2 are all positive.

To this end, the overall control structure of PCSMC (29)-(32) is depicted by Fig. 3. Here, only the d-axis current i_{d} and mechanical rotation speed ω_{m} need to be measured. Finally, the obtained control inputs are modulated through sinusoidal pulse width modulation (SPWM) [33].

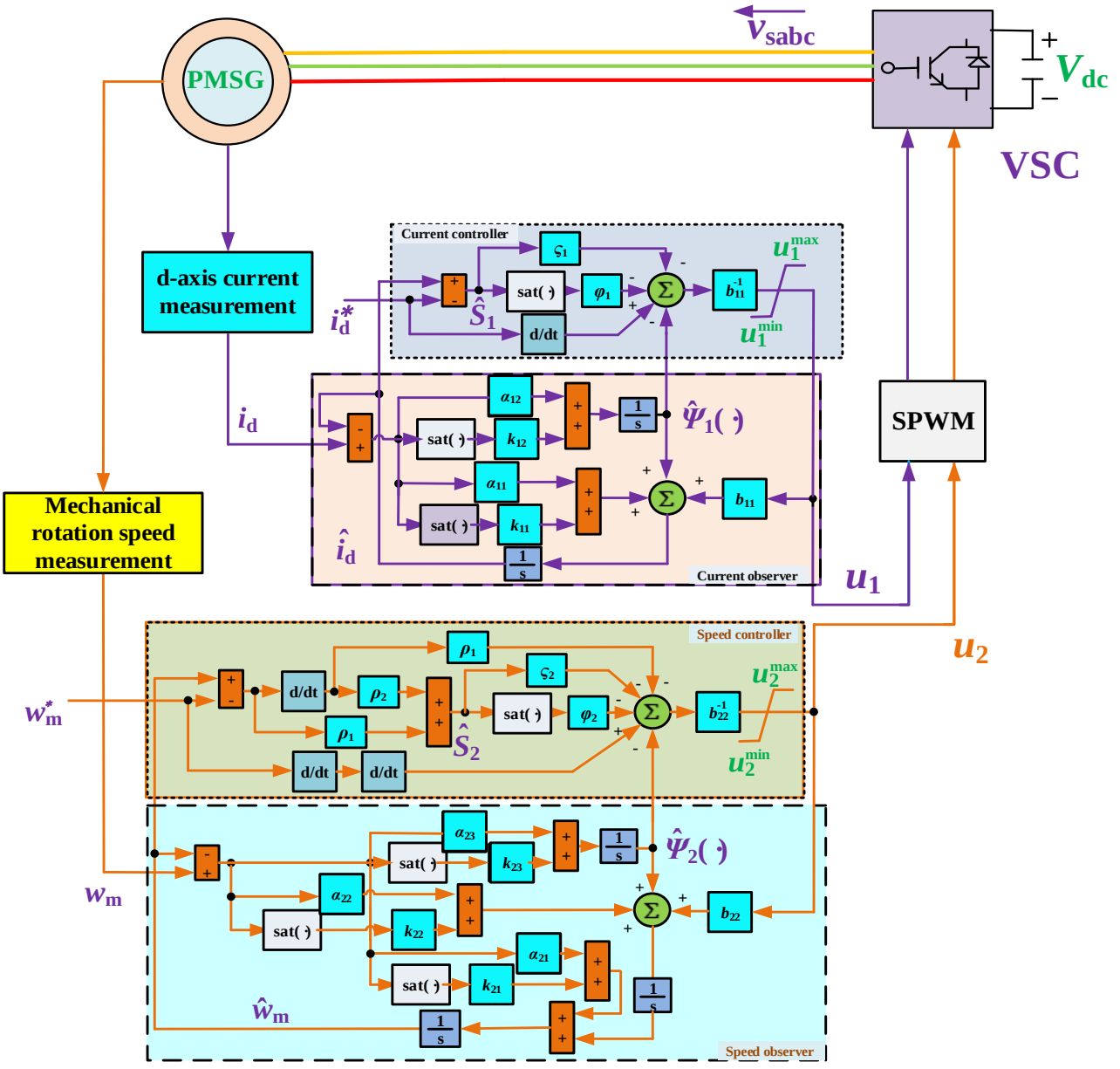

Fig. 3 *The overall PCSMC framework of PMSG.*

5. Case Studies

The MPPT performance of PCSMC is compared to both conventional VC [8] and SMC [22], under four scenarios, i.e., (a) Step change of wind speed; (b) Low-turbulence stochastic wind speed; (c) High-turbulence stochastic wind speed; and (d) PMSG parameter uncertainties. Moreover, control inputs u_1 and u_2 are limited among [-1.0, 1.0] per unit (p.u.). In addition, the PMSG system parameters and PCSMC parameters are tabulated in Table 1 and Table 2, respectively. Simulation environment is based on Matlab/Simulink 2016a.

Table 1. System parameters of PMSG

PMSG rated power	P_{base}	2 MW	**Field flux**	K_{e}	136.25 V·s/rad
Radius of wind turbine	R	39 m	**Pole pairs**	p	11
d-axis stator inductance	L_{d}	3.75 mH	**Air density**	ρ	1.205 kg/m^3
q-axis stator inductance	L_{q}	5.5 mH	**Rated wind speed**	v_{wind}	12 m/s
Total inertia	J_{tot}	10000 kg·m^2	**Stator resistance**	R_{s}	50 $\mu\Omega$

Table 2. PCSMC parameters

d-axis current control	$b_{11}=-1500$	$\boldsymbol{\varsigma_1}$=10	$\boldsymbol{\varphi_1}$= 8	$\boldsymbol{\alpha_{11}}$= 40	$\boldsymbol{\alpha_{12}}$= 400
	$k_{11}=15$	$k_{12}=600$	$\epsilon_o=0.2$	$\epsilon_{\text{c}}=0.2$	
Mechanical rotation speed control	b_{22}=−3000	ς_2=15	φ_2=12	$\rho_1=150$	$\rho_2=1$
	α_{21}=30	α_{22}=300	α_{23}=1000	k_{21}=20	k_{22}=600
	k_{23}=6000				

5.1. Step change of wind speed

Four consecutive step changes of wind speed starting at 8 m/s and ending at 12 m/s (10 m/s^2 rate) is applied to emulate a gust while a step change of d-axis current is studied. The wind speed curve and MPPT performance are provided in Fig. 4. One can readily observe that VC has the largest active power overshoots and the slowest tracking rate in comparison to that of SMC and PCSMC. In contrast, PCSMC is able to keep the power coefficient closest to its optimum, thus the maximum power can be extracted from wind. Moreover, it verifies that the d-axis current is fully decoupled from mechanical rotor speed, in which PCSMC can track the d-axis current reference with the highest rate.

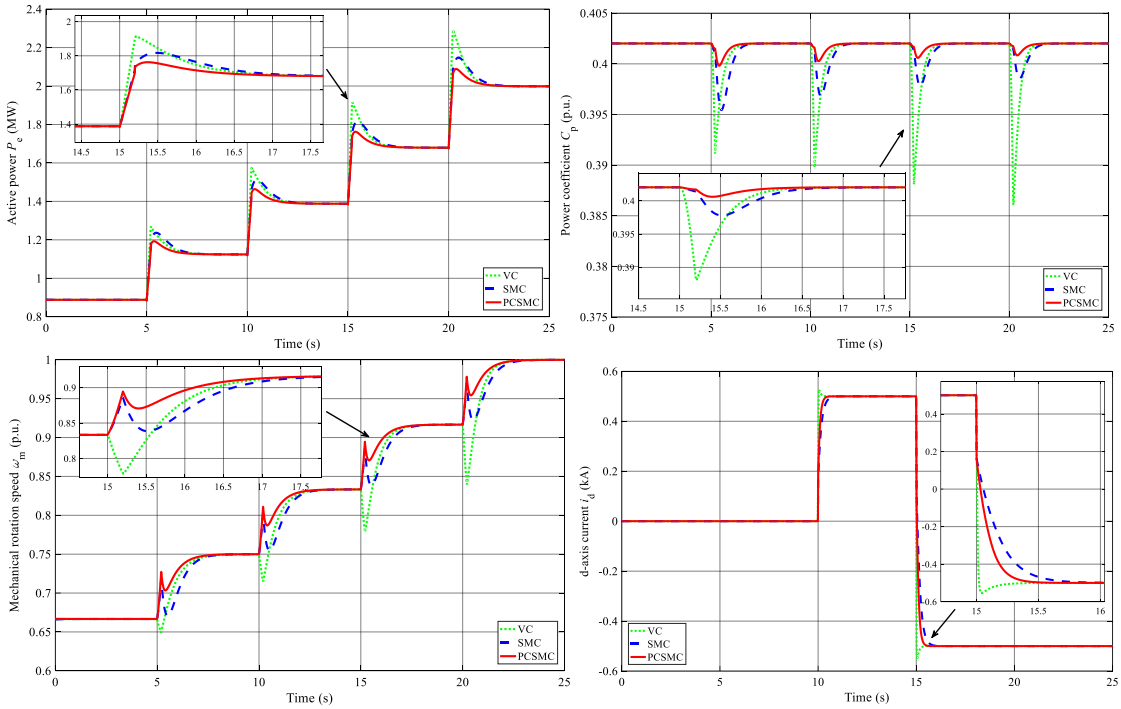

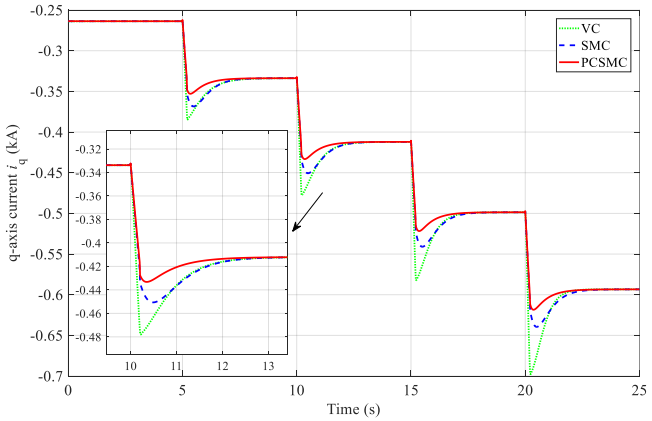

Fig. 4 *System responses and control costs obtained under a step change of wind speed between 8 m/s to 12 m/s.*

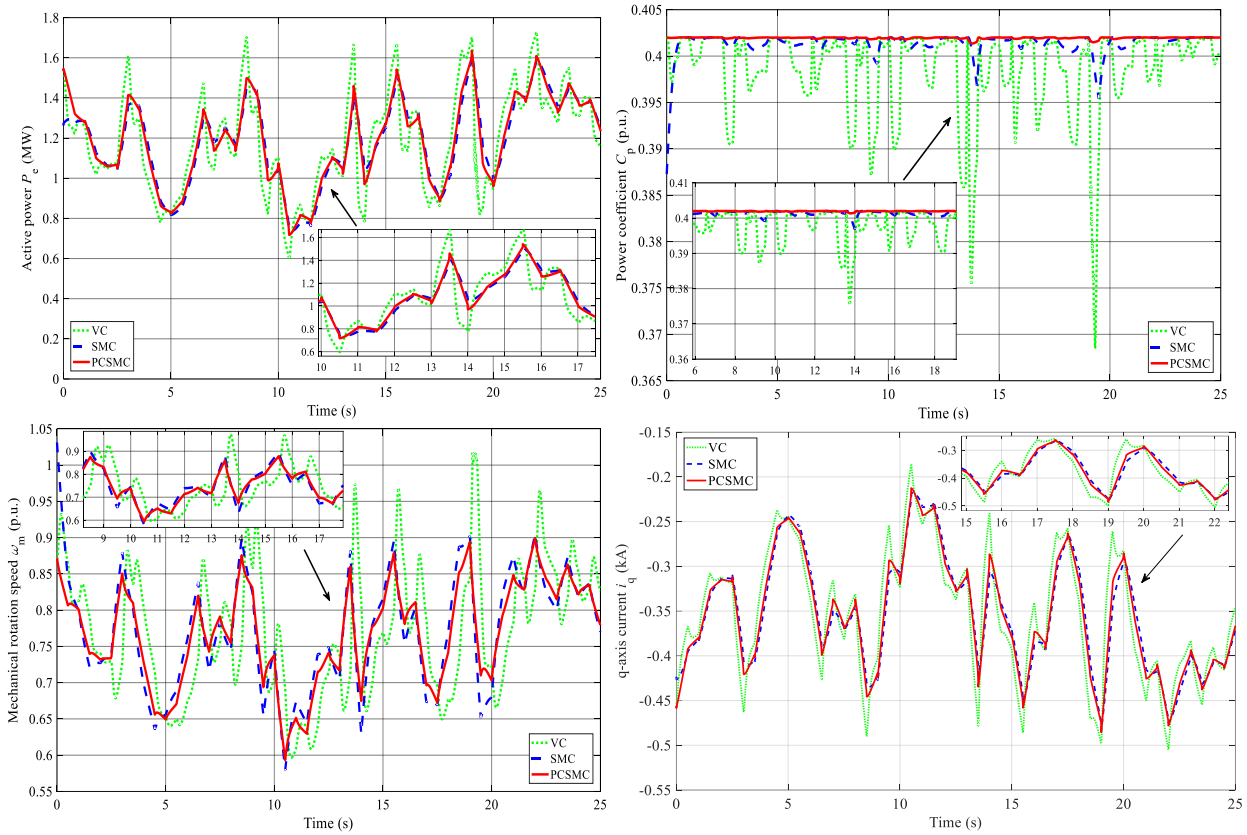

Fig. 5 *System responses obtained under a low-turbulence stochastic wind speed between 7 m/s to 11 m/s.*

5.2. Low-turbulence stochastic wind speed

A low-turbulence stochastic wind speed varying from 7 m/s to 11 m/s, which simulates a general wind variation, is applied. The system responses are provided in Figure 5, which demonstrates that the power coefficient of PCSMC is the optimal among all as such wind speed randomness can be rapidly estimated by SMSPO in the real-time, and then fully compensated by the PCSMC. In addition, the control performance of VC varies dramatically at different wind speed, this is due to the fact that PID control cannot maintain a global control consistency.

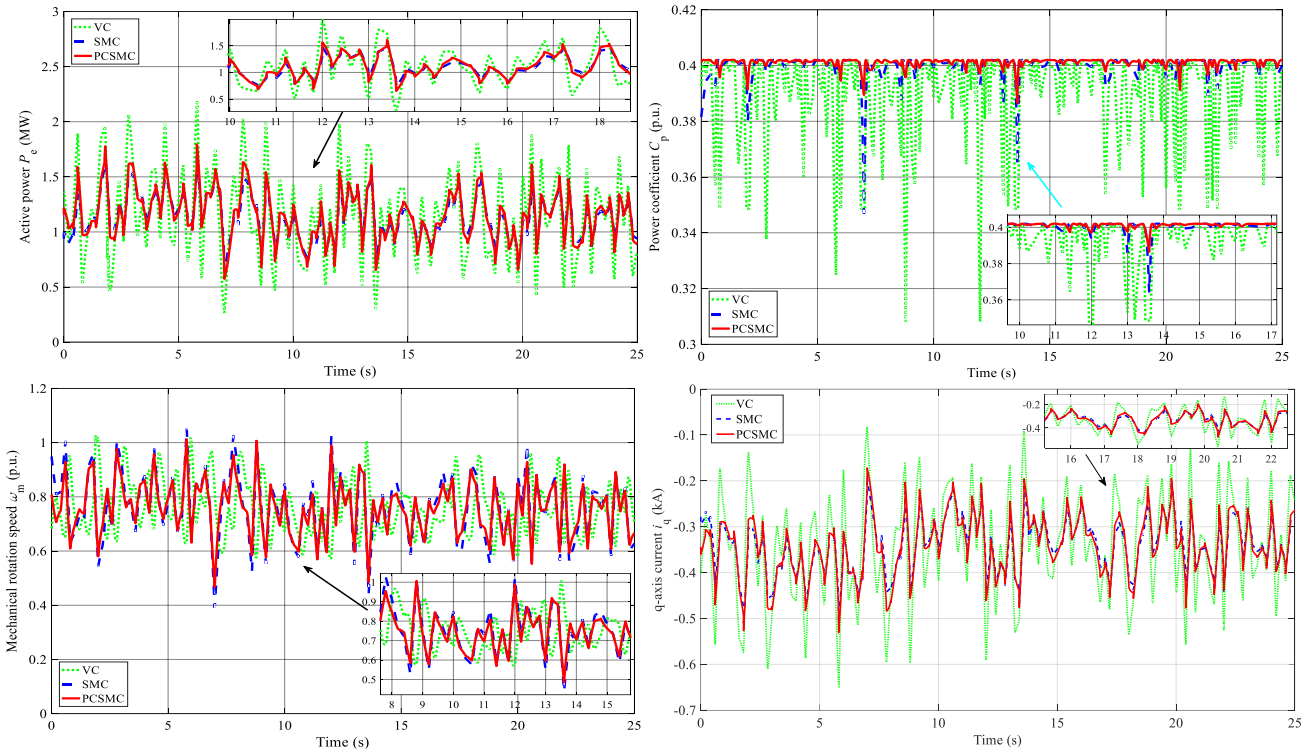

Fig. 6 *System responses obtained under a high-turbulence stochastic wind speed between 6 m/s to 12 m/s.*

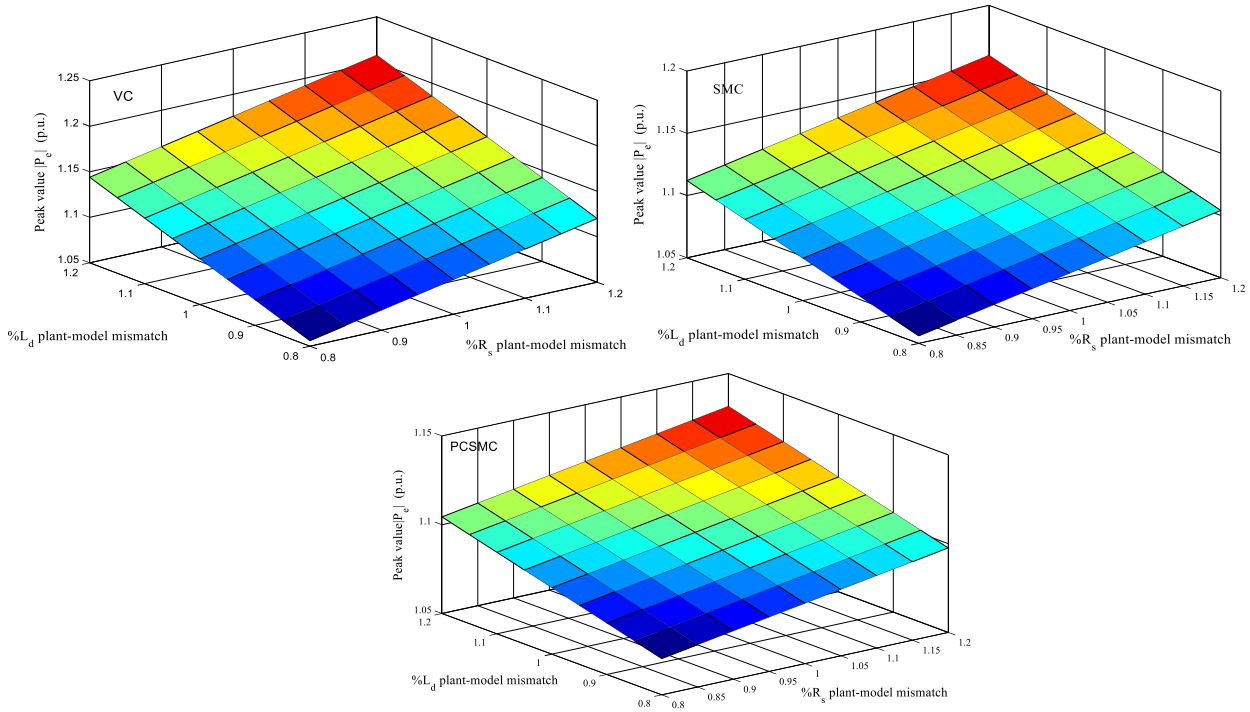

Fig. 7 *Peak value variation of active power |Pe| obtained under a 1 m/s step change of wind speed from the rated value (12 m/s) with 20% uncertainties of stator resistance Rs and d-axis inductance Ld*

5.3. High-turbulence stochastic wind speed

To mimic severe wind speed variations, e.g., high mountains, coastal areas, etc. [34-36]. A high-turbulence stochastic wind speed among 6 m/s to 12 m/s is adopted for MPPT evaluation, which results are illustrated in Fig. 6. It is clear that PCSMC can generate the highest power. Again, VC performs the worst among the three methods. Note that SMC needs much higher control costs than that of PCSMC due to its over-conservativeness.

5.4. PMSG Parameter Uncertainties

In order to investigate the robustness in the presence of PMSG parameter uncertainties, a series of stator resistance R_s and d-axis inductance L_d uncertainties with ±20% variation are investigated, in which a 1 m/s step change of wind speed is studied. Figure 7 depicts that the variation of $|P_e|$ (which means the variation of active power compared to the one before the step) is

16.1%, 10.4%, 7.8% by VC, SMC, and PCSMC respectively. As PCSMC can fully compensate the parameter uncertainties in real-time, it has the strongest robustness against generator parameter uncertainties among all approaches.

5.5. Comparative Studies

Integral of absolute error (IAE) indices [37,38] of each controller required in the first three cases are given in Table 3, where $\mathrm{IAE}_x = \int_0^T |x - x^*| \, \mathrm{d}t$. The simulation time T = 25 s. One can readily find that PCSMC has the lowest IAE indices (in bold) in all scenarios. More specifically, its $\mathrm{IAE}\omega_\mathrm{m}$ obtained in low-turbulence stochastic wind speed is just 47.86% and 55.57% of that of VC and SMC, respectively.

Table 3. IAE indices of different controllers obtained in different cases (p.u.).

Case	Step change of wind speed	Low-turbulence stochastic wind speed	High-turbulence stochastic wind speed
Controller	IAE index $\mathrm{IAE}\omega_\mathrm{m}$ of mechanical rotation speed		
VC	1.46E-01	6.77E-01	9.87E-01
SMC	1.08E-01	5.83E-01	8.41E-01
PCSMC	**7.65E-02**	**3.24E-01**	**3.24E-01**
Controller	IAE index IAE_{id} of d-axis current		
VC	1.58E-02	6.48E-03	8.21E-03
SMC	1.31E-02	4.17E-03	6.55E-03
PCSMC	**9.85E-03**	**2.42E-03**	**3.96E-03**

At last, the control costs of all controllers required in three cases are demonstrated in Figure 8. Here, control costs mean the the overall integral of the sum of control outputs, e.g., $\int_0^T (|u_1| + |u_2|) \, \mathrm{d}t$. It is obvious to observe that PCSMC owns the lowest control costs thanks to the full compensation of perturbation in real-time thus the inherent over-conservativeness of SMC can be effectively avoided.

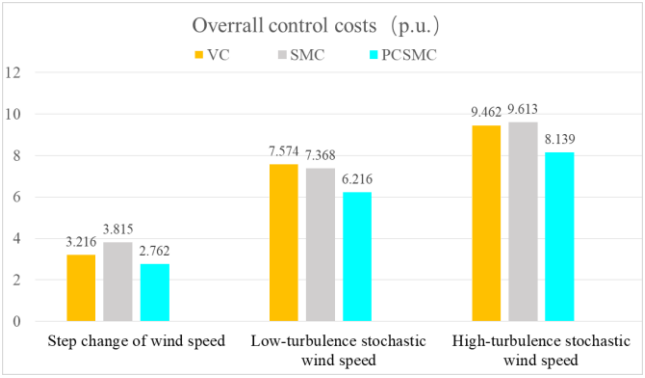

Fig. 8 *Overall control costs required by different controllers under three cases.*

6. HIL Experiment

HIL experiment has been used to validate the effectiveness and implementation feasibility of advanced PMSG control systems [39-41].

An HIL experiment using dSpace is carried out, as shown in Fig. 9 and Fig. 10, respectively. In particular, PCSMC (32) is embedded on DS1104 board with a sampling frequency f_c=1 kHz. Meanwhile, PMSG system (21) is implemented on DS1006 board with a limit sampling frequency f_s= 50 kHz [34].

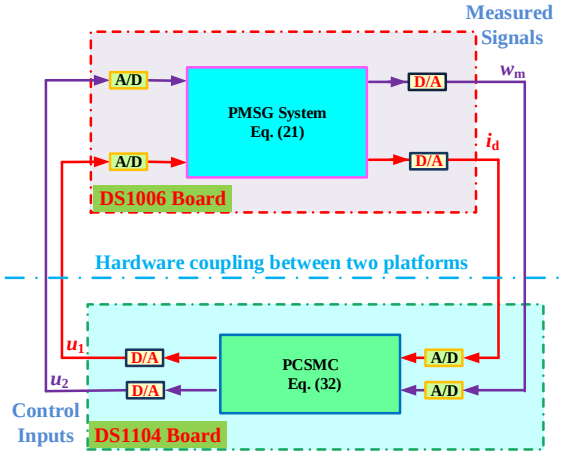

Fig. 9 *The configuration of HIL experiment.*

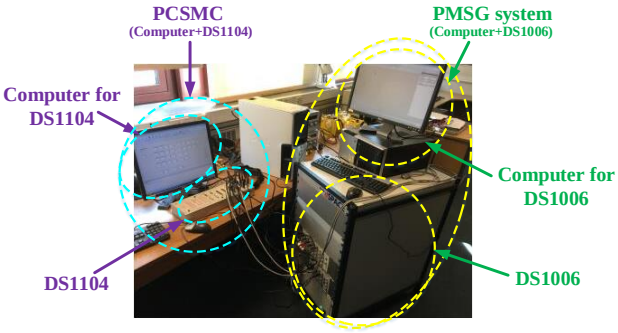

Fig. 10 *The hardware platform of HIL experiment.*

6.1 HIL results: Step change of wind speed

Figure 11 compares the system responses obtained by both simulation and HIL experiment under step change of wind speed change. One can find that simulation results and HIL experiment results are quite similar to each other.

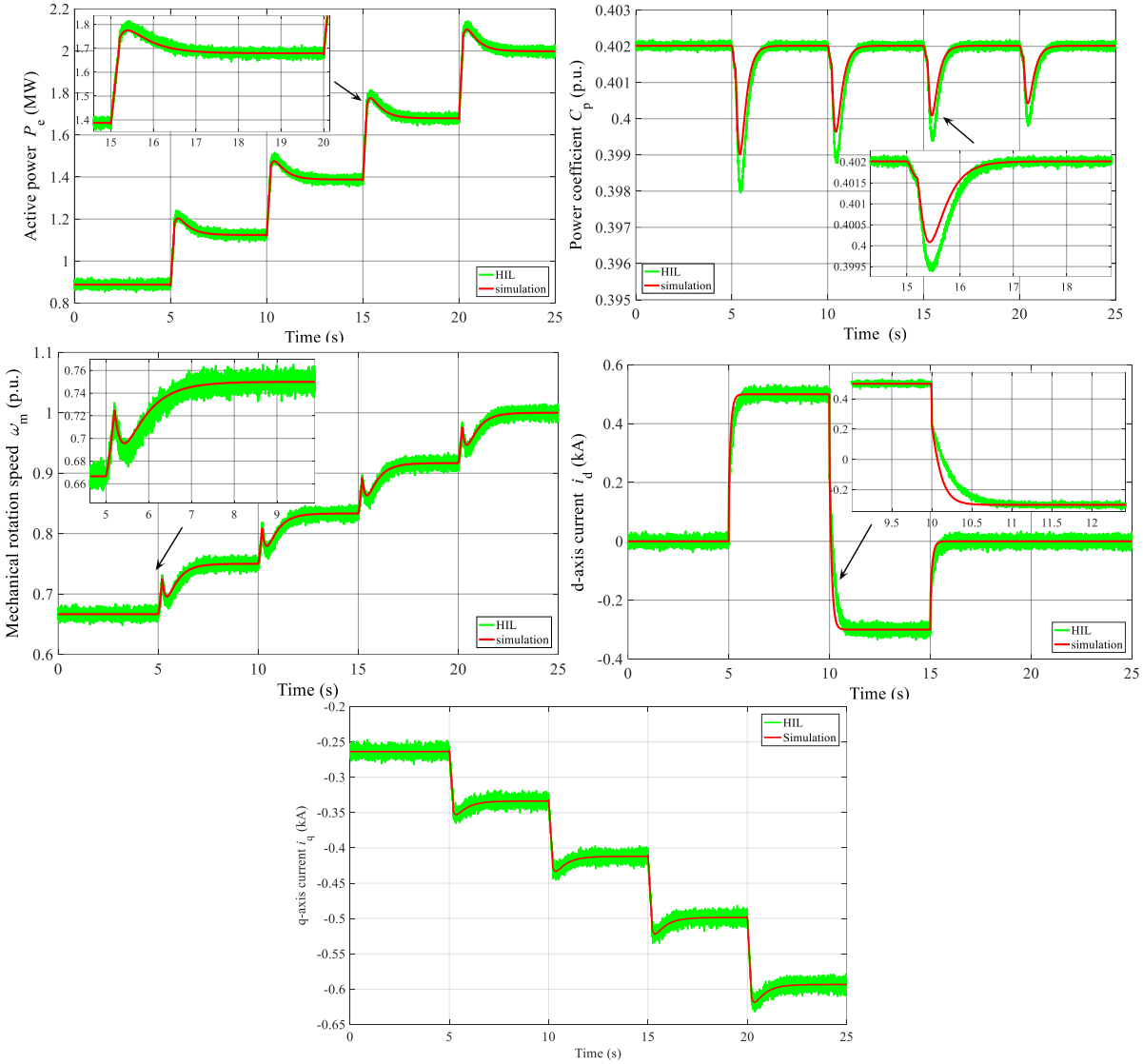

Fig. 11 *Simulation and HIL experiment results obtained under step change of wind speed.*

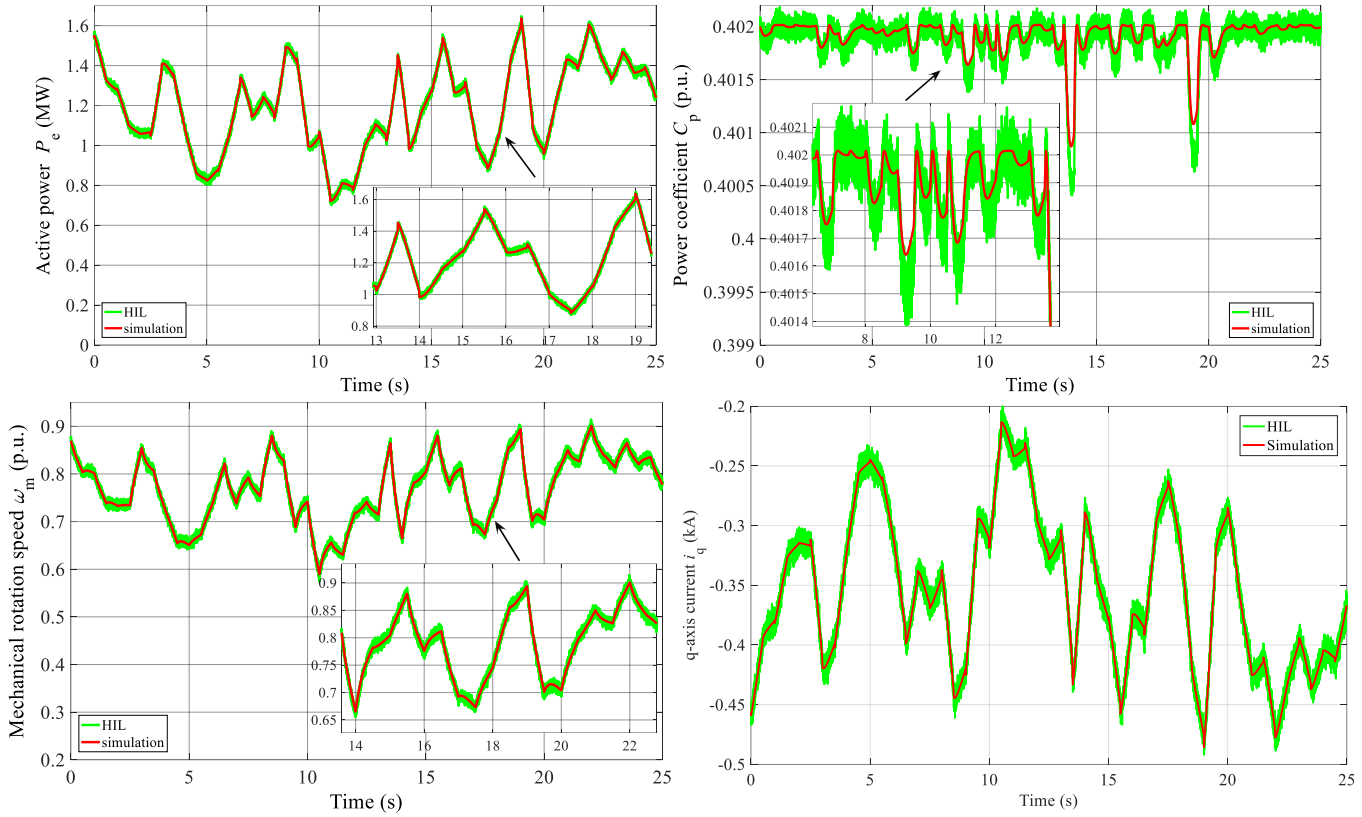

Fig. 12 *Simulation and HIL experiment results obtained under low-turbulence stochastic wind speed.*

6.2 HIL results: Low-turbulence stochastic wind speed

Under the same scenario of low-turbulence stochastic wind speed, Figure 12 illustrates that the MPPT performance of HIL experiment and simulation matches each other very well.

6.3 HIL results: High-turbulence stochastic wind speed

The same high-turbulence stochastic wind speed is applied, while Fig. 13 presents the obtained results. One can observe that the curves of HIL experiment and simulation are very close to each other.

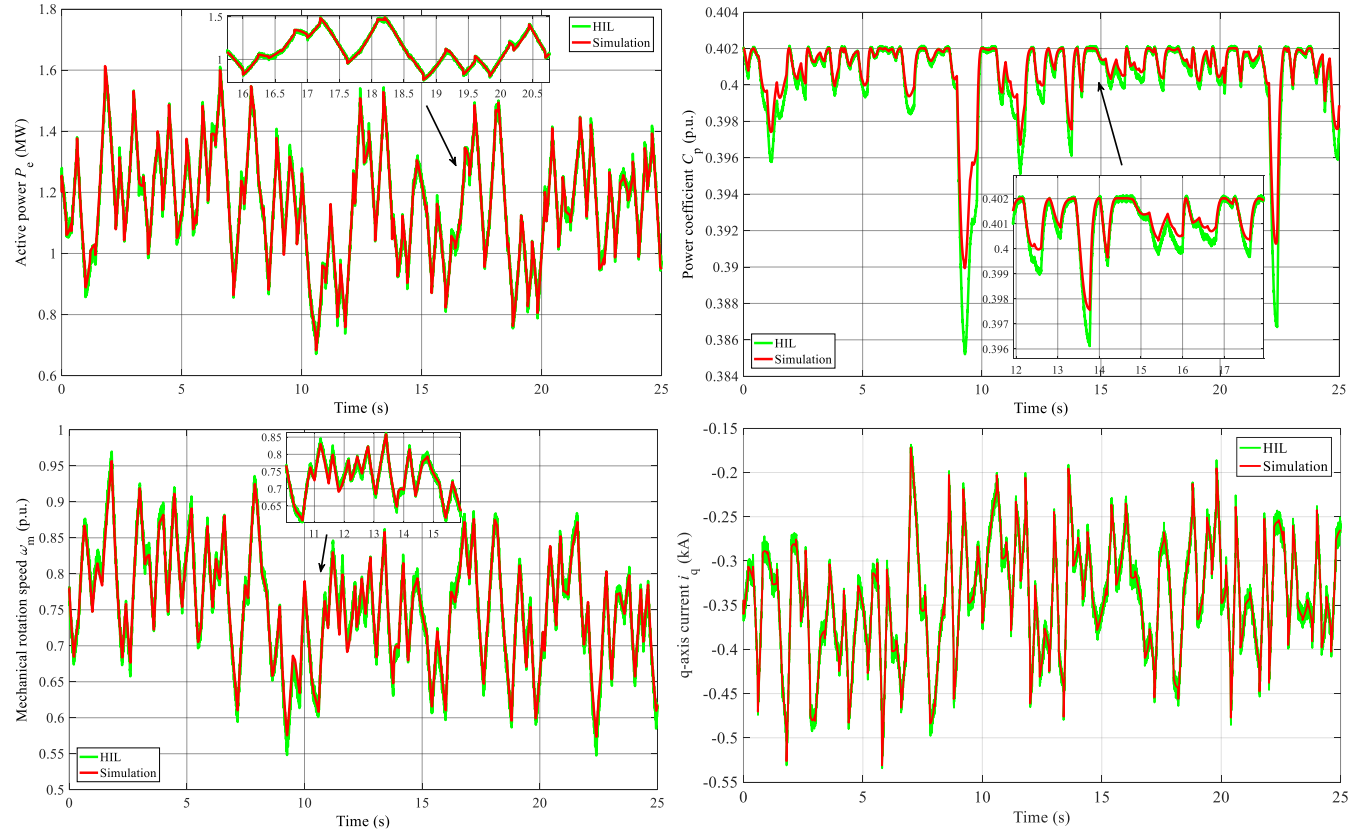

Fig. 13. *Simulation and HIL experiment results obtained under high-turbulence stochastic wind speed.*

To this end, the results difference between simulation and HIL experiment is mainly due to the followings:

• *Uncertain measurement disturbances and noises in the HIL experiment*: It is not considered in the simulation and mainly leads to the consistent oscillations of the HIL experiment results;

• *Discretization of the HIL experiment and sampling holdin*g: It usually brings additional amount of tracking errors in comparison to continuous control in simulation;

• *Time delay of the real-time controll*er: The exact time relay is very difficult to know in HIL experiment. It usually leads to control performance degradation.

7. Conclusions

This paper develops PCSMC strategy for PMSG to achieve MPPT under different wind profiles. The main finds/contributions can be concluded as

(1) An SMSPO is employed to rapidly estimate the combinatorial effect of PMSG nonlinearities, uncertain parameters, unmodelled dynamics, and stochastic wind speed variation online. Then, the estimated perturbation is fully cancelled by SMC to realize a globally consistent control performance, together with significant robustness thanks to the sliding-mode mechanism;

(2) The over-conservativeness of SMC is effectively avoided through using the real-time estimate of perturbation. Hence, proper control costs can be realized with an improved error tracking performance;

(3) PCSMC does not require an accurate PMSG model while only the mechanical rotation speed and d-axis current need to be measured. Moreover, their control are fully decoupled by the design of diagonal control gain matrix;

(4) Case studies verify that PCSMC can achieve a global control consistency under various wind profile, together with the lowest overall control costs;

(5) dSpace based HIL experiment validates the implementation feasibility of PCSMC.

Future studies will be focused on the following two directions:

(a) Apply PCSMC on the grid-side VSC to enhance the fault ride-through (FRT) capability of PMSG;

(b) Undertake HIL experiment on a real PMSG to further validate the implementation feasibility of PCSMC.

Acknowledgments

The authors gratefully acknowledge the support National Natural Science Foundation of China (51477055, 51667010, 51777078), and Yunnan Provincial Basic Research Project-Youth Researcher Program (2018FD036).

References

[1] Liao, S.W., Yao, W., Han, X.N., Wen, J.Y., Cheng, S.J.: 'Chronological operation simulation framework for regional power system under high penetration of renewable energy using meteorological data', *Applied Energy*, 2017, **203**, pp. 816-828.

[2] Yang, B., Yu, T., Zhang, X.S., Li, H.F., Shu, H.C., Sang, Y.Y., Jiang, L.: 'Dynamic leader based collective intelligence for maximum power point tracking of PV systems affected by partial shading condition', *Energy Conversion and Management*, 2019, **179**, pp. 286-303.

[3] Shen, Y., Yao, W., Wen, J.Y., He, H.B.: 'Adaptive wide-area power oscillation damper design for photovoltaic plant considering delay compensation', *IET Generation, Transmission and Distribution*, 2017, **11**, (18), pp. 4511-4519.

[4] Yang, B., Zhang, X.S., Yu, T., Shu, H.C., Fang, Z.H.: 'Grouped grey wolf optimizer for maximum power point tracking of doubly-fed induction generator based wind turbine', *Energy Conversion and Management*, 2017, **133**, pp. 427-443

[5] Yang, B., Yu, T., Shu, H.C., Zhang, X.S., Qu, K.P., Jiang, L.: 'Democratic joint operations algorithm for optimal power extraction of PMSG based wind energy conversion system', *Energy Conversion and Management* , 2018, **159**, pp. 312-326

[6] Tripathi, S.M., Tiwari, A.N., Singh, D.: 'Grid-integrated permanent magnet synchronous generator based wind energy conversion systems: A technology review', *Renewable and Sustainable Energy Reviews*, 2015, **51**, pp. 1288-1305

[7] Kumar, D., Chatterjee, K.: 'A review of conventional and advanced MPPT algorithms for wind energy systems', *Renewable and Sustainable Energy Reviews*, 2016, **55**, pp. 957-970

[8] Shehata, E.G.: 'A comparative study of current control schemes for a direct-driven PMSG wind energy generation system', *Electric Power Systems Research*, 2017, **143**, pp. 197-205

[9] Xing, B., Gao, W.J.: 'Innovative computational intelligence: A rough guide to 134 clever algorithms', Springer International Publishing, Switzerland, 2014

[10] Hasanien, H.M., Muyeen, S.M.: 'Design optimization of controller parameters used in variable speed wind energy conversion system by genetic algorithms', *IEEE Transactions on Sustainable Energy*, 2012, **3**, (2), pp. 200-208

[11] Kim, Y.S., Chung, I.Y., Moon, S.I.: 'Tuning of the PI controller parameters of a PMSG wind turbine to improve control performance under various wind speeds', *Energies*, 2015, **8**, pp. 1406-1425

[12] Rukslin, Haddin, M., Suprajitno, A.: 'Pitch angle controller design on the wind turbine with permanent magnet synchronous generator (PMSG) base on firefly algorithms (FA)', *Technology of Information and Communication, IEEE*, Semarang, Indonesia, 5-6 Aug. 2016, pp. 13-17

[13] Chen, J., Jiang, L., Yao, W., Wu, Q.H.: 'A feedback linearization control strategy for maximum power point tracking of a PMSG based wind turbine', *International Conference on Renewable Energy Research and Applications*, Madrid, Spain, 20-23 October 2013, pp. 79-84

[14] Howlader, A.M., Urasaki, N., Yona, A., Senjyu, T., Saber, A.Y.: 'Design and implement a digital $H\infty$ robust controller for a MW-class PMSG-based grid-interactive wind energy conversion system', *Energies*, 2013, **6**, pp. 2084-2109

[15] Zhang, X., Huang, C., Hao, S., Chen, F., Zhai, J.: 'An improved adaptive-torque-gain MPPT control for direct-driven PMSG wind turbines considering wind farm turbulences', *Energies*, 2016, **9**, 977

[16] Daili, Y., Gaubert, J.P., Rahmani, L.: 'Implementation of a new maximum power point tracking control strategy for small wind energy conversion systems without mechanical sensors', *Energy Conversion and Management*, 2015, **97**, pp. 298-306

[17] Ikram, M.H., Mohamed, W.N., Najiba, M.B.: 'Predictive control strategies for wind turbine system based on permanent magnet synchronous generator', *ISA Transactions*, 2016, **62**, pp. 73-80

[18] Fantino, R., Solsona, J., Busada, C.: 'Nonlinear observer-based control for PMSG wind turbine', *Energy*, 2016, **113**, pp. 248-257

[19] Jafari, A., Shahgholian, G.: 'Analysis and simulation of a *sliding mode controller* for mechanical part of a doubly-fed induction generator-based wind turbine', *IET Generation Transmission & Distribution*, 2017, **11**, (10), pp. 2677-2688
[20] Yin, X.X., Lin, Y.G., Li, W., Gu, Y.J., Liu, H.W., Lei, P.F.: 'A novel fuzzy integral sliding mode current control strategy for maximizing wind power extraction and eliminating voltage harmonics', *Energy*, 2015, **85**, pp. 677-686
[21] Seyed, M.M., Maarouf, S., Hani, V., Handy, F.B., Mohsen, S.: 'Sliding mode control of PMSG wind turbine based on enhanced exponential reaching law', *IEEE Transactions on Industrial Electronics*, 2016, **63**, (10), pp. 6148-6159
[22] Fernando, V., Roberto, D.F.: 'Multiple-input-multiple-output high-order sliding mode control for a permanent magnet synchronous generator wind-based system with grid support capabilities', *IET Renewable Power Generation*, 2015, **9**, (8), pp. 925-934
[23] Yazici, I., Yaylaci, K.E.: 'Maximum power point tracking for the PMSG based WECS by using the discrete-time integral sliding mode controller with a chattering free reaching law', *IET Power Electronics*, 2017, doi:10.1049/iet-pel.2017.0232
[24] Phan, D.H., Huang, S.D.: 'Super-twisting sliding mode control design for cascaded control system of PMSG wind turbine', *Journal of Power Electronics*, 2015, **15**, (5), pp. 1358-1366
[25] Yan, J., Lin, H., Feng, Y., Guo, X., Huang, Y., Zhu, Z.Q.: 'Improved sliding mode model reference adaptive system speed observer for fuzzy control of direct-drive permanent magnet synchronous generator wind power generation system', *IET Renewable Power Generation*, 2013, **7**, (1), pp. 28-35
[26] Uehara, A., Pratap, A., Goya, T., Senjyu, T., Yona, A., Urasaki, N., Funabashi, T.: 'A coordinated control method to smooth wind power fluctuations of a PMSG-based WECS', *IEEE Transactions on Renewable Energy*, 2011, **26**, (2), pp. 550-558
[27] Yang, B., Jiang, L., Wang, L., Yao, W., Wu, Q.H.: 'Nonlinear maximum power point tracking control and modal analysis of DFIG based wind turbine', *International Journal of Electrical Power & Energy Systems*, 2016, **74**, pp. 429-436
[28] Yang, B., Hu, Y.L., Huang, H.Y., Shu, H.C., Yu, T., Jiang, L.: 'Perturbation estimation based robust state feedback control for grid connected DFIG wind energy conversion system', *International Journal of Hydrogen Energy*, 2017, **42**, (33), pp. 20994-21005
[29] Liu, Y., Wu, Q.H., Zhou, X.X., Jiang, L.: 'Perturbation observer based multiloop control for the DFIG-WT in multimachine power system', *IEEE Transactions on Power Systems*, 2014, **29**, pp. 2905-2915
[30] Yang, B., Sang, Y.Y., Shi, K., Yao, W., Jiang, L., Yu, T.: 'Design and real-time implementation of perturbation observer based sliding-mode control for VSC-HVDC systems', *Control Engineering Practice*, 2016, **56**, pp. 13-26
[31] Jiang, L., Wu, Q.H., Wen, J.Y.: 'Nonlinear adaptive control via sliding-mode state and perturbation observer', *IEE Proceedings of Control Theory Applications*, 2002, **149**, pp. 269-277
[32] Yang, B., Yu, T., Shu, H.C., Zhu, D.N., An, N., Sang, Y.Y., Jiang, L.: 'Perturbation observer based fractional-order sliding-mode controller for MPPT of grid-connected PV inverters: design and real-time implementation', *Control Engineering Practice*, 2018, **79**, pp. 105-125.
[33] Wu, F.J., Sun, D.Y., Duan, J.D.: 'Diagnosis of single-phase open-line fault in three-phase PWM rectifier with LCL filter', *IET Generation Transmission & Distribution*, 2016, **10**, (6), pp. 1410-1421
[34] Yang, B., Yu, T., Shu, H.C., Zhang, Y.M., Chen, J., Sang, Y.Y., Jiang, L.: 'Passivity-based sliding-mode control design for optimal power extraction of a PMSG based variable speed wind turbine', *Renewable Energy*, 2018, **119**, pp. 577-589
[35] Yang, B., Yu, T., Shu, H.C., Dong, J., Jiang, L.: 'Robust sliding-mode control of wind energy conversion systems for optimal power extraction via nonlinear perturbation observers', *Applied Energy*, 2018, **210**, pp. 711-723
[36] Liu, J., Wen, J. Y., Yao, W., Long, Y.: 'Solution to short-term frequency response of wind farms by using energy storage systems', *IET Renewable Power Generation*, 2016, **10**, (5), pp. 669-678
[37] Yao, W., Jiang, L., Wen, J.Y., Wu, Q.H., Cheng, S.J.: 'Wide-area damping controller for power system inter-area oscillations: a networked predictive control approach', *IEEE Transactions on Control Systems Technology*, 2015, **23**, (1), pp. 27-36
[38] Shen, Y., Yao, W., Wen, J. Y., He, H. B., Chen, W. B.: 'Adaptive supplementary damping control of VSC-HVDC for interarea oscillation using GrHDP', *IEEE Transactions on Power Systems*, 2018, **33**, (2), pp. 1777-1789
[39] Li, H., Steurer, M., Shi, K.L., Woodruff, S., Zhang, D.: 'Development of a unified design, test, and research platform for wind energy systems based on hardware-in-the-Loop real-time simulation', *IEEE Transactions on Industrial Electronics* 2006, **53**, (4), pp. 1144-1151
[40] Hasanzadeh, A., Edrington, C.S., Stroupe, N., Bevis, T.: 'Real-time emulation of a high-speed microturbine permanent-magnet synchronous generator using multiplatform hardware-in-the-loop realization', *IEEE Transactions on Industrial Electronics*, 2014, **61**, (6), pp. 3109-3118
[41] Huerta F., Tello R.L., Prodanovic, M.: 'Real-time power-hardware-in-the-loop implementation of variable-speed wind turbines', *IEEE Transactions on Industrial Electronics*, 2017, **64**, (3), pp. 1893-1904